ADVANCED FUNCTIONAL MATERIALS
www.afm-journal.de

Multimodal Label-Free Monitoring of Adipogenic Stem Cell Differentiation Using Endogenous Optical Biomarkers

*Nishir Mehta, Shahensha Shaik, Alisha Prasad, Ardalan Chaichi, Sushant P. Sahu, Qianglin Liu, Syed Mohammad Abid Hasan, Elnaz Sheikh, Fabrizio Donnarumma, Kermit K. Murray, Xing Fu, Ram Devireddy, and Manas Ranjan Gartia**

Stem cell-based therapies carry significant promise for treating human diseases. However, clinical translation of stem cell transplants for effective treatment requires precise non-destructive evaluation of the purity of stem cells with high sensitivity (<0.001% of the number of cells). Here, a novel methodology using hyperspectral imaging (HSI) combined with spectral angle mapping-based machine learning analysis is reported to distinguish differentiating human adipose-derived stem cells (hASCs) from control stem cells. The spectral signature of adipogenesis generated by the HSI method enables identifying differentiated cells at single-cell resolution. The label-free HSI method is compared with the standard techniques such as Oil Red O staining, fluorescence microscopy, and qPCR that are routinely used to evaluate adipogenic differentiation of hASCs. HSI is successfully used to assess the abundance of adipocytes derived from transplanted cells in a transgenic mice model. Further, Raman microscopy and multiphoton-based metabolic imaging is performed to provide complementary information for the functional imaging of the hASCs. Finally, the HSI method is validated using matrix-assisted laser desorption/ionization-mass spectrometry imaging of the stem cells. The study presented here demonstrates that multimodal imaging methods enable label-free identification of stem cell differentiation with high spatial and chemical resolution.

1. Introduction

Mesenchymal stem cells (MSCs) can be sourced from bone marrow,[1] umbilical cord,[2] and adipose tissue.[3] Human adipose-derived stem cells (hASCs) have been well established as a potential tool for tissue engineering and regenerative medicine applications due to their easy access and lack of ethical issues associated with embryonic stem cells. The hASCs properties of self-renewal, multipotency for differentiation along various cell lineages, and the ability to secrete cytokines and chemokines have been extensively reported during the past decade.[4] Adipogenic stem-cell culture requires differentiation times ranging from 9 to 21 days and is expensive. Analysis methods using destructive and invasive techniques such as chemical staining assay, real-time quantitative polymerase chain reaction (qPCR), western blotting assay, and immunostaining to assess the stem cells prevent the re-use of priceless differentiated cells after analysis as these methods require cell lysis, chemical staining, and cell fixation.[5] Label-free non-invasive techniques will facilitate researchers to investigate the cells before clinical transplantation as a quality check and allowing them to perform temporal analysis, thus maximizing the chance of the cell transplant. Hence, label-free approaches capable of probing the stem cells in their native state are required.

Another concern for the clinical translation of hASCs is the formation of teratomas – where a small number of undifferentiated stem cells after transplantation in vivo may lead

N. Mehta, A. Prasad, A. Chaichi, S. P. Sahu, S. M. A. Hasan, E. Sheikh, R. Devireddy, M. R. Gartia
Department of Mechanical and Industrial Engineering
Louisiana State University
Baton Rouge, LA 70803, USA
E-mail: mgartia@lsu.edu

S. Shaik
Division of Basic Pharmaceutical Sciences
College of Pharmacy
Xavier University of Louisiana
New Orleans, LA 70125, USA

Q. Liu, X. Fu
LSU AgCenter
School of Animal Sciences
Louisiana State University
Baton Rouge, LA 70803, USA

F. Donnarumma, K. K. Murray
Department of Chemistry
Louisiana State University
Baton Rouge, LA 70803, USA

The ORCID identification number(s) for the author(s) of this article can be found under https://doi.org/10.1002/adfm.202103955.

DOI: 10.1002/adfm.202103955

to tumor formation.[6] It is estimated that ≈10^4 undifferentiated cells are sufficient to produce teratomas when implanted in vivo.[6b] Also, for effective treatment, implantation of about ≈10^9 cells is required.[7] That means an effective method should be capable of discerning differences in the cell at a level of 1 in 10^5 cells (0.001%). Flow cytometry is capable of identifying undifferentiated cells in a cell population at a rate of >1 in 10^3 (>0.1%).[8] Therefore, the sensitivity of flow cytometry is not sufficient to evaluate stem cell purity for transplants. The gold standard method for checking the purity of cells is to transplant them into SCID mice to check for tumor formation.[9] But this method takes about 3 months, is expensive, cells might become non-retrievable and is not quantitative. Therefore, a robust, low-cost, sensitive, and fast method of detecting differentiated stem cells will provide enormous advantages in stem cell therapy.

Previously, several label-free approaches such as electrochemical impedance spectroscopy (EIS),[10] Fourier transform infrared spectroscopy (FTIR),[11] Raman spectroscopy,[12] and coherent anti-stokes Raman spectroscopy (CARS)[13] were utilized to investigate the progression of stem cell differentiation. Although promising, EIS measurements cannot identify the differentiation rate in stem cells as there are no significant changes in the impedance signals between the cell membrane and electrodes during the progression of differentiation.[14] Due to the strong absorption of IR light in water, FTIR spectra of cells maintained under physiological conditions can be distorted and are challenging to carry out. Further, the spatial resolution of FTIR (>5 µm) is typically smaller than that of Raman imaging (≈250 nm). Thus, FTIR cell imaging lacks single-cell resolution and requires complex sample preparation that involves sample drying or fixing.[15] In addition to being expensive, CARS microscopy is limited by capturing a single vibrational mode at a time. Further, due to the mixing of nonresonant background (contribution from $\chi^{(3)}$) with resonant vibrational peaks, CARS has limited sensitivity in detecting weak Raman bands. Additionally, the CARS signal has a quadratic relationship with the concentration of the molecules. Hence, it is difficult to detect molecules with low concentrations using CARS.[15] Raman imaging can provide the spectroscopic signatures of the component of stem cells (nucleus, protein, lipids, cytoplasm, etc.) with high resolution and specificity.[16] Raman spectroscopy has been used to track adipogenesis,[5,13,17] osteogenesis,[5,18] and other stem cell lineages.[16,19] However, precise identification of changes in the chemical cues during stem cell differentiation from the Raman spectra obtained from the cellular components (e.g., cytoplasm, nucleus, proteins) are challenging. This is because, significant changes in the cellular components are not expected during stem cell differentiation[5] while significant changes in structure are expected. During Raman analysis of stem cells, auto fluorescence of the cellular components and supporting cell substrates in the fingerprint region obscure the Raman peaks. In addition, photo-damage due to the laser is a limitation for long-term Raman imaging of the cells.[20]

This paper demonstrates the hyperspectral imaging (HSI) method to non-invasively probe the adipogenic differentiation in hASCs (**Figure 1**). The HSI spectral signature is based on the fact that the scattering and absorption of light within stem cells

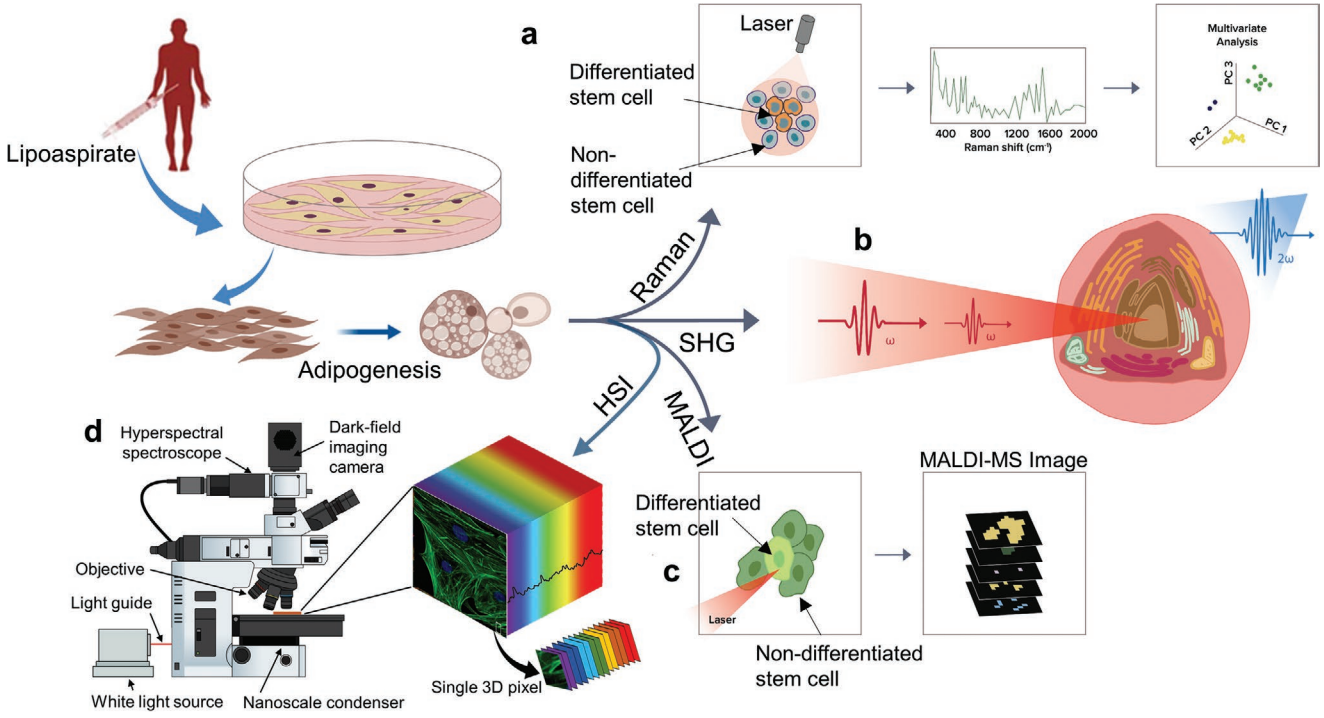

Figure 1. Schematic overview of quantitative label-free imaging implemented at the single-cell level. a) Label-free monitoring of human adipose-derived stem cell (hASCs) differentiation to adipogenic stem cells using Raman spectroscopy; b) Metabolic imaging using second harmonic generation (SHG) of stem cells to detect differentiated stem cells from control cells; c) MALDI-mass spectrometry imaging of lipid in differentiated stem cells; d) Schematic arrangement showing the hyperspectral imaging (HSI) system. The HSI system captures the spatial and spectral signature at each pixel of the image to form the data cube.

is a function of morphological and molecular changes occurring during the differentiation process.[21] We collected more than fifteen million scattering spectral signatures using HSI. We analyzed them using the spectral angle mapping (SAM)-machine learning method to build a library that provided the "signature" of adipogenesis. The technique was successfully demonstrated to distinguish differentiated stem cells from control stem cells at an early stage. The HSI results were compared with traditional cell characterization methods (Oil Red O, qPCR), multiphoton imaging, and Raman spectroscopy. Further, the HSI results were validated by performing MALDI-MS imaging of the differentiated and control stem cells. The multimodal imaging approach using HSI and other spectroscopic methods implemented here provides a new tool for label-free assessment of stem cells.

2. Results and Discussion

We utilized HSI to perform label-free chemical imaging to distinguish differentiated hASCs from non-differentiated control cells. Three other label-free modalities (Raman, SHG, MALDI-MS) were used to validate the HSI study and to obtain chemically selective information of the various components of the differentiated stem cells (Figure 1). Figure S4 (Supporting Information) shows the characterization of stem cell marker expression of ASCs at passage 2 (P2) determined by flow cytometer (BD FACS Calibur). The representative dot plots for the positive and negative stem cell markers are shown in Figure S4a–e (Supporting Information). The % expression data is shown in the table (Figure S4f, Supporting Information), which indicates that the positive stem cell markers CD90, CD73, CD105, CD29, CD44 are above 90%, whereas negative stem cells CD146, CD34, CD45, and CD31 are less than 1% in expression. This clearly suggests that the cells used in this study are indeed adult stem cells derived from adipose tissue. The adipogenic potential of the stem cells was confirmed by staining the differentiated cell population with phalloidin (for cytoskeletal/actin) and Hoechst (nucleus) stains (**Figure 2**a–c). To probe the adipogenesis, we stained the cells with Nile red and Hoechst (Figure 2d) stains. The globular lipid droplet structures within the cells are clearly visible on day 9, representing matured adipocytes (Figure 2d). This accumulation of lipid droplets are is a hallmark of the adipogenic differentiation process.[13,22] To further confirm the adipogenic lineage, we investigated the gene expression level of adiponectin,[23] leptin,[24] and PPARg,[25] which were found to be associated with the promotion of adipogenic differentiation. The mRNA fold change of these adipogenic genes was calculated and normalized to cyclophilin B gene by the $2^{-\Delta\Delta CT}$ method.[26] All the gene expression levels increased for hASCs cultured for

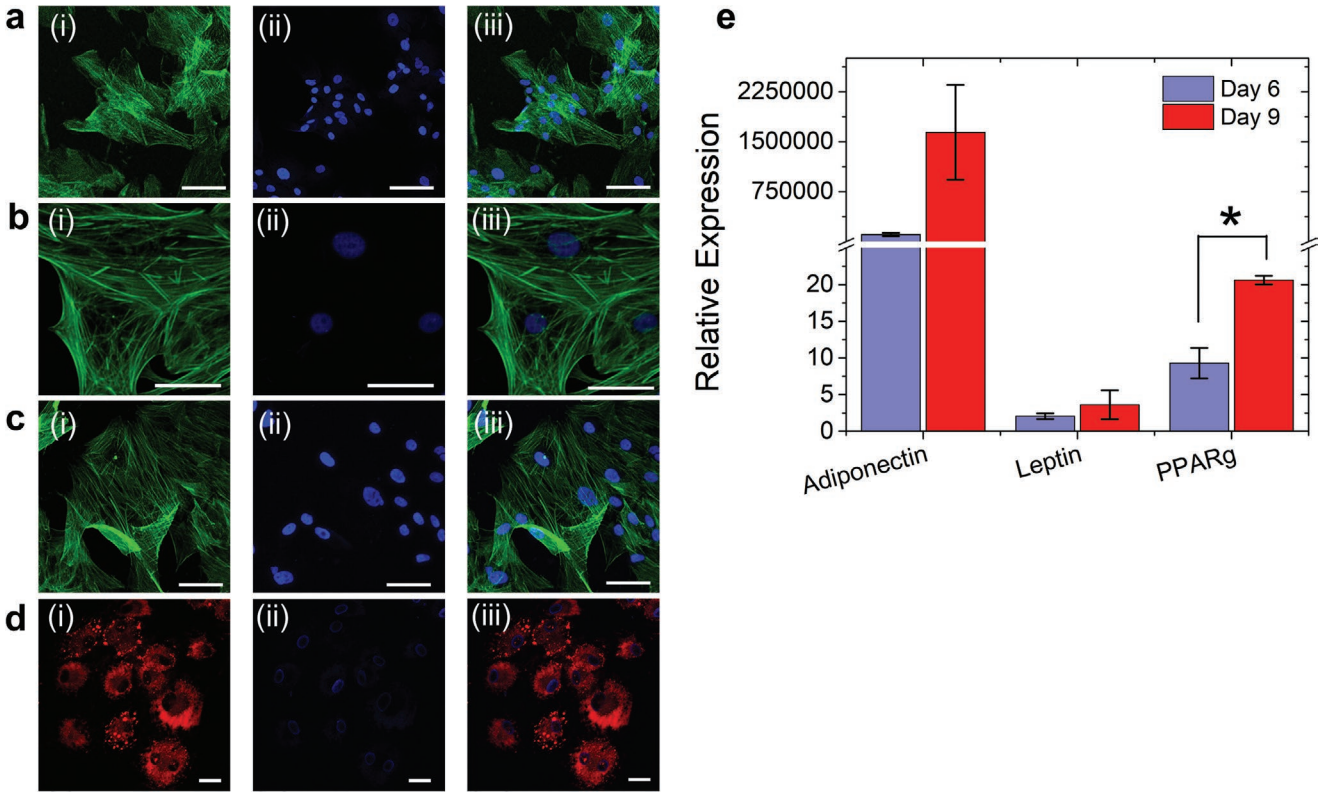

Figure 2. Representative cytochemical image of hASCs and gene expression profile. Confocal fluorescence images of cells cultured in adipogenic media for a) 1, b) 3, c) 6, and d) 9 days. The sub-cellular component of each images (scale = 20 μm) are shown for (i) cytoplasm, (ii) nucleus, and (iii) merged. The matured adipocytes (globular lipid droplets) are clearly seen on day 9 with the Nile red-stained cells; e) Relative gene expression profiles of adiponectin, leptin, and PPARg for stem cells incubated in adipogenic media for 6, and 9 days. Relative expression was normalized to cyclophilin B. The results show the average of three independent donor samples, and the error bars represent standard deviation. $^*P < 0.05$, calculated using two-tailed Student's *t*-test.

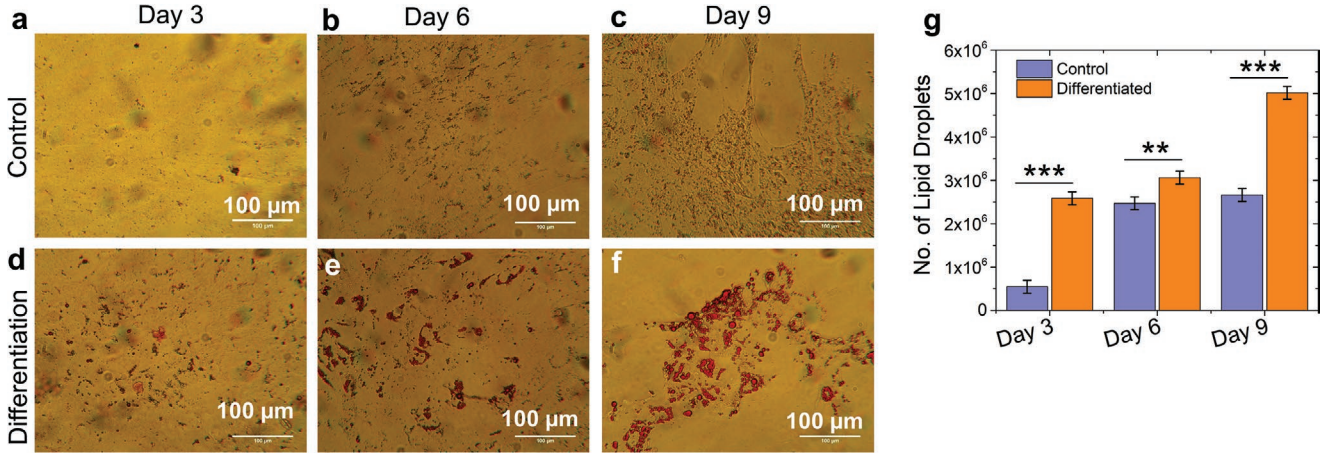

Figure 3. Confirmation of differentiation of hASCs using Oil Red O staining. Comparison of bright field images of Oil Red O staining assay of hASCs for a–c) control (with stromal media) and d–f) differentiated (with adipogenic media) cells. The cells cultured in stromal and adipogenic media for 3, 6, and 9 days are shown; g) Comparison of the number of lipid droplets in differentiated and control cells on days 3, 6, and 9. All the experiments were performed in triplicate. $^{*}P < 0.05$, $^{**}P < 0.01$, $^{***}P < 0.001$, two-tailed Student's *t*-test.

nine days in adipogenic media then six days culture. Especially, the expression level of PPARg, a key regulator for adipocyte differentiation,[27] is increased significantly ($P < 0.05$) on day 9 compared to day 6 (Figure 2e). The increase in the expression level of these genes demonstrates the successful induction of adipogenesis and correlates with the growth of lipid droplets in hASCs with the progression of time.

The results of conventional histochemical staining of lipids with Oil Red O are shown in **Figure 3**. There is a progressive increase in lipid content with time (day 3 vs day 9). hASCs cultured in adipogenic media (Figure 3d–f) showed significant higher ($P < 0.001$) lipid content compared to the stromal media (Figure 3a–c). At least a 4-fold increase in the number of droplets on day 9 compared to day 3 was observed for the differentiated cells. These experiments performed over large imaging areas (10x magnification) correlated well with the fluorescence imaging experiments (in Figure 2) performed over relatively smaller areas (63x magnification).

After the conventional validation of success in the differentiation of hASCs into the adipogenic lineage, we characterized adipogenic differentiation using label-free dark-field microscopy combined with hyperspectral imaging (HSI). Analysis of the acquired dark-field images of biological specimens involves preprocessing of the HSI data cubes, identifying regions of interest and selecting reference spectra of endogenous optical markers to build libraries, and then applying classification algorithms to generate meaningful information. There were a total of 30 fields of view (FOV) from $n = 3$ independent donors captured for both the control and the differentiated samples at days 3, 6, and 9. Each FOV resulted in a generation of 484 416 pixels, and in turn, each pixel consisting of spatial information and spectral information in the visible near-infrared (VIR) range. That is, the analysis of each image consists of 484416 spectra and a total of 14.5×10^6 spectra for the current study. HSI showed much higher resolution and contrast (≈50 nm per pixel) for the lipid droplets without external probes compared to fluorescence and Oil Red O imaging. The stem cells cultured in stromal media (control cells) showed a much smaller number of lipid droplets (**Figure 4**a–c) compared to the adipogenic media (Figure 4d–f). Further, the size and number of droplets in control cells did not change much with time (Figure 4h). In contrast, the size of droplets in the differentiated cells progressively grew with time (Figure 4g,h). Surprisingly, the number of droplets in the differentiated cells decreases with time (Figure 4h), possibly due to the coalescence of smaller droplets to form larger droplets. The size of the droplets also changed during the differentiation period. For example, on day 3, most lipid droplets were <2 µm^2, whereas, on day 9, all of the lipid droplets were >20 µm^2 (Figure 4g). All of the lipid droplets found in control cells remained <2 µm^2 (Figure 4h, inset). One of the essential advantages of HSI over Oil red O staining and fluorescence imaging is that HSI showed sensitivity toward detecting smaller droplets (early adipogenesis) even on day 3, which are not efficiently imaged using conventional methods (Nile red, Oil red O).

To extract HSI spectral signatures of the differentiated stem cells, we analyzed and found 6 distinct end members (EM) using the SAM method (**Figure 5**a). The characteristic spectral profiles of each endmember are shown in Figure 5b–g (each endmember is pseudo-colored for visualization). The location of each EM is shown schematically in Figure 5h. EM-1 originates from the membranes of the lipid droplets (Figure 5b) with their spectral peaks at $\lambda = 796$ nm. EM-2 ($\lambda = 586$ nm) and EM-3 ($\lambda = 721$ nm) represent the spectra from the species surrounding the lipid droplets (Figure 5d) and matrix between droplets (Figure 5c), respectively. EM-4, with the peak at $\lambda = 663$ nm, comes from the cytoplasm of the differentiated cell (Figure 5e). EM-5 represents the spectra extracted from the fatty esters of the oil well since no peak bands were present in the profile (Figure 5f). This was an expected outcome due to the refractive index matching of adipogenic oil-wells with microscopy oil used in the dark-field objective lens. EM-6 ($\lambda = 838$ nm) corresponds to smaller lipid droplets (Figure 5g). Spectral profiles of EM 1–6 were registered as the reference library in this study and were used in the SAM algorithm. Data presented in Figure 5i confirms the spectral distinctiveness of

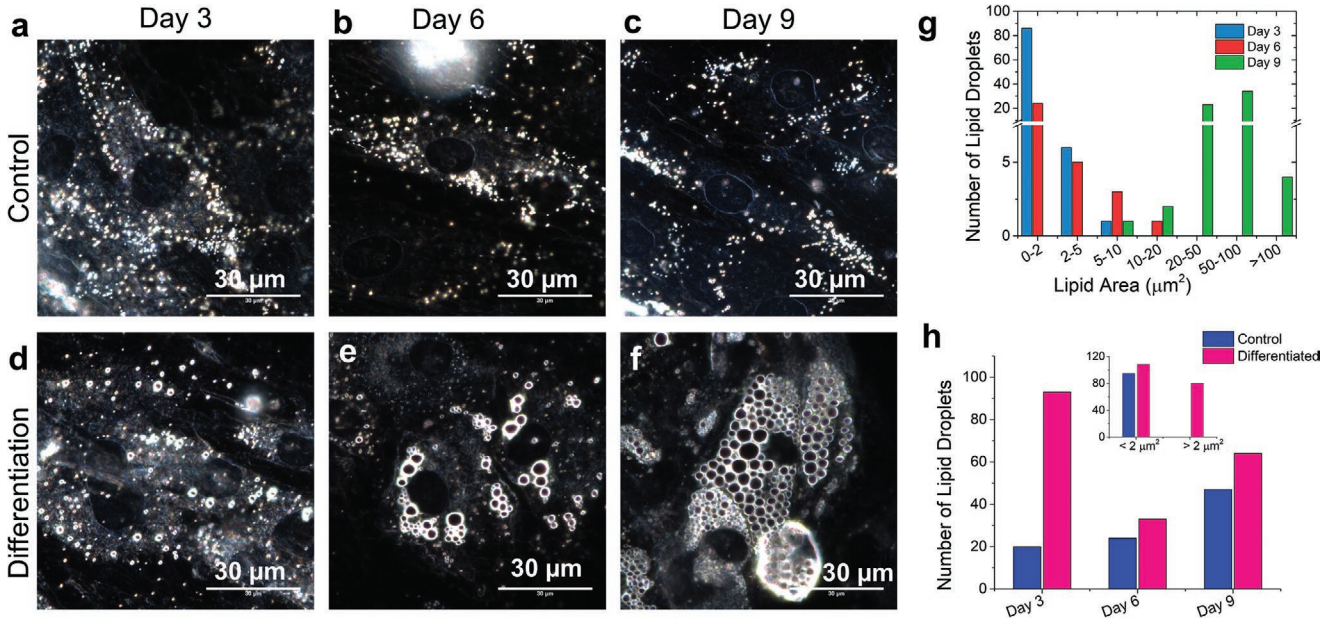

Figure 4. Representative dark-field images showing the morphology of single hASCs cell. Comparison of dark-field images of stem cells in a–c) stromal, d–f) adipogenic media for 3, 6, and 9 days. A progressive increase in the number of larger lipid droplets is visible in the differentiated cells with time compared to control stem cells; g) Comparison of size of lipid droplets on different days in differentiated cells. The lipid droplets increased in size with time; h) The distribution of number of lipid droplets for the control and differentiated cells on day 3, 6, and 9. The inset shows that the lipid droplets found in the control cells are primarily of size < 2 μm^2.

the reference library primary components. One of the most widely used methods to check dataset distinctiveness is principal component analysis (PCA). When PCA is used to check reference library discriminative features, it preserves the variance in high-dimensional space yet reduces redundant information[28] in the bands of HSI images, as shown in Figure 5j. This further confirms that the HSI spectra result from scattering due to distinctive species and structures within the cells.

The spectral library identified earlier was implemented to perform spectral mapping (**Figure 6**) on control and differentiated cells. Figure 6 provides histograms reporting quantitative percentage classification using the SAM algorithm for each endmember at different time points. The percentage classification describes how many pixels in a particular image (out of ≈500 000 total pixels) belong to a specific endmember. It should be noted that each pixel is composed of spatial as well as spectral information. Among the six spectra, EM-5 represents the main contribution (≈4%) toward the total scattering of the differentiated cells on day 9 (Figure 6e). This is not surprising since EM-5 is due to the lipid droplets, and by day 9, most of the cell area is occupied by the lipid droplets. It is evident from the histogram that the differentiated stem cells can be clearly distinguished from the control cells onward of day 6 culture using HSI. The differentiated hASCs on day 9 were found to be significantly different ($P < 0.001$) than the control cells at the same time point while using EM-1 (Figure 6a), EM-3 (Figure 6c), EM-5 (Figure 6e), and EM-6 (Figure 6f) classification spectra. On day 6, the analysis showed significant differences ($P < 0.05$) between control and differentiated stem cells for all of the endmembers. The percentage of pixels in the "matched" output on day 3 culture of control and differentiated cells on day 3 was not significant. The percentage classification of endmembers associated with lipid wall periphery (EM-3) and lipid droplets (EM-5) was more significant compared to that of other endmembers, which is consistent with lipid droplet formation during the progression of adipogenesis shown earlier (Figure 3). SAM classification is insensitive to variation in illumination intensity, and hence it is handy for clinical stem cell therapy. The different rates of cellular metabolism and the differences in the cell morphologies during adipogenic differentiation result in differences in the scattering spectra compared to that from control cultures. Thus, HSI provides an alternative quantitative label-free method to monitor hASCs differentiation with minimum sample preparation.

To validate the HSI results and identify the molecular origin of each endmember, we performed MALDI-MS imaging and LC-MS of the control and differentiated hASCs.[29] A comparison of positive ion mode MALDI mass spectra for hASCs cultured for 9 days in adipogenic (differentiated stem cells) and stromal media (control stem cells) is shown in **Figure 7**a. A representative MALDI image of a differentiated cell showing the distribution of FA and DG is shown in Figure 7b,e. The corresponding dark-field image of the cells is shown in Figure 7d. The higher molecular weight peaks ($m/z > 1200$) seen in the control cell spectrum are absent in differentiated stem cells. Because we were mainly interested in profiling lipids, we restricted our analysis to lipidomics. Ganglioside (GD3 d18:1/24:1 m/z 1592.881) was not observed in the differentiated stem cells but is seen in the control cells. Gangliosides are generally responsible for proliferation and transmembrane signaling.[30] They reside in the lipid raft of the membrane[31] (Figure 7f) and are found to be lower with adipogenesis,[32] which is consistent with our observation. In stem cells cultured in stromal media, we found many glycerophospholipids such

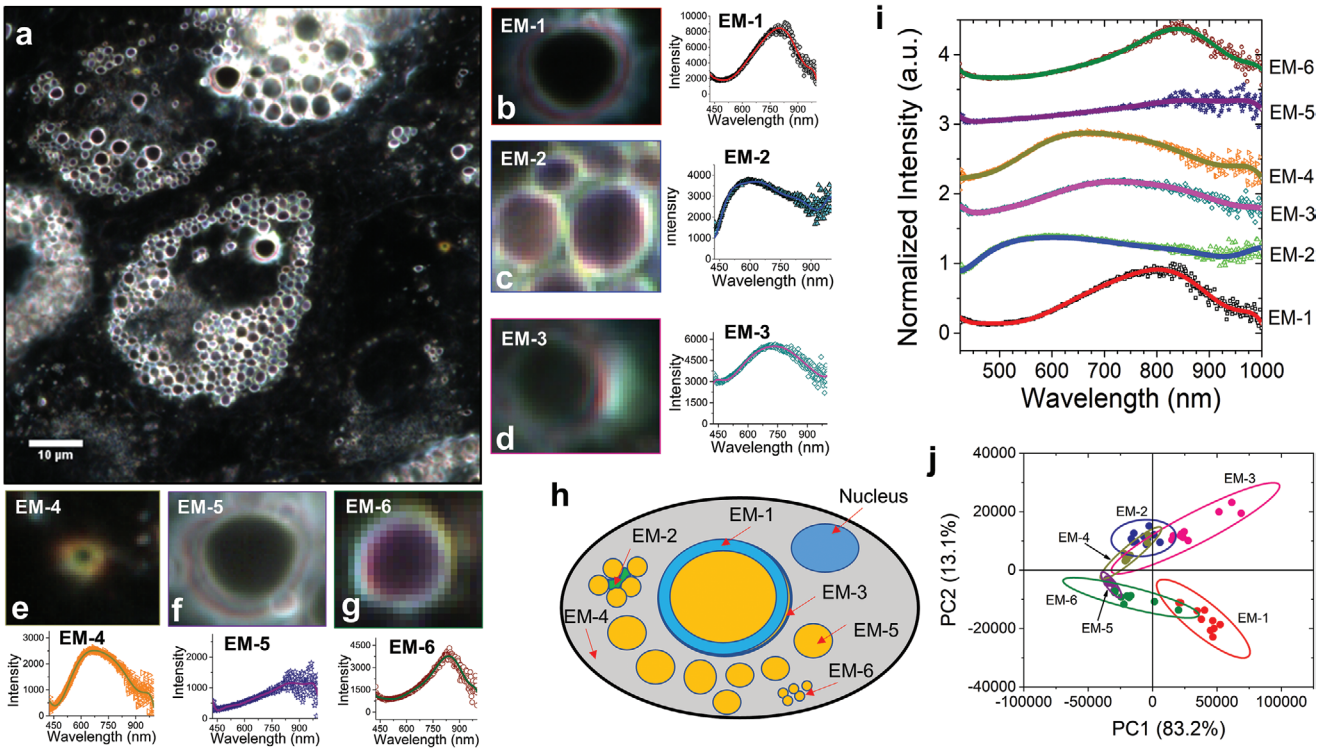

Figure 5. Representative hyperspectral imaging (HSI) of the differentiated hASCs and analysis of their optical biomarkers. a) HSI of differentiated stem cells (day 9) with the mapped spectral endmembers using spectral angle mapper (SAM) analysis. The spectral library was composed of 6 end members (EM-1 to 6). b–g) The zoomed-in images of each endmember are shown. The colored area in the images is indicative of the match with the spectral profiles. The spectral signature of the end members in the wavelength range 450 – 950 nm is shown next to the respective end member images; h) Schematic figure showing the location inside the cells from which the spectral signature corresponding to each endmembers is originating; i) Comparison of the spectral signature of the six end members; j) Principal component analysis (PCA) score plot of the six endmembers for the first two principal components (PC1 vs PC2). For each endmember, 10 different HSI images were analyzed. Images were acquired using 100x, image size 75 µm x 75 µm, number of samples, $n = 3$ corresponding to three separate donors.

as phosphatidylcholine (PC 28:2;O2, *m/z* 706.474; PC 34:2, *m/z* 758.573; PC 30:3;O3, *m/z* 786.437), phosphatidylserine (PS 30:1, *m/z* 706.474; PS 35:4, *m/z* 808.459), phosphatidylethanolamine (PE 37:2, *m/z* 758.573; PE O-42:4, *m/z* 832.623), phosphatidic acid (PA O-41:0, *m/z* 761.644), cardiolipins (CL 70:6, *m/z* 1463.943; CL 74:1, *m/z* 1492.127; CL 72:5, *m/z* 1493.975; CL 78:2, *m/z* 1546.168), and various sphingolipids (ceramide, Cer 44:0;O4, *m/z* 734.66; HexCer 32:3;O2, *m/z* 706.474; gangliosides, Hex(4)-HexNAc(2)-Cer 34:2;O2, *m/z* 1592.891; Hex(2)-NeuAc(2)-Cer 42:2;O2, *m/z* 1592.881). Cardiolipins prevent lipid droplet formation by increasing energy consumption.[33] This could explain why cardiolipins were found in control cells but not in the differentiated stem cells. Mammalian cell membranes are rich in PC and PE. Alteration in PC and PE can lead to changes in lipid droplet size and their formation.[34] In the MALDI-MS of differentiated cells we observed many hallmarks of lipid droplets such as glycerolipids (TG 52:4, *m/z* 855.747; DG 31:1, *m/z* 553.487; MG O-21:0;O, *m/z* 441.333), sterol lipids (ST 27:1, *m/z* 435.348; ST 28:1, *m/z* 439.333; ST 27:2;O4;S, *m/z* 551.246), and fatty acyls (FA 26:1, *m/z* 465.342). It is well known that di(acyl|alkyl)glycerols (DG) facilitate membrane fusion promoting protein and lipid droplet formation.[35] Tri(acyl|alkyl)glycerols (TG) are also abundantly found inside the lipid droplets (Figure 7c). We found PG 40:4 (*m/z* 827.578), prominent mitochondrial phospholipids, responsible for cell growth and promoter of anaerobic metabolism.[36] Further, the overcrowded adipocytes produce cytokines and adipokines due to stress.[37] This is consistent with the observation of ceramides (Cer 38:0;O3, *m/z* 650.55), which are generally implicated in apoptosis.[38] The full list of lipids found in this study is in the supporting information (Tables S1 and S2, Supporting Information). A total of 439 lipids (112 in negative ion mode and 327 in positive ion mode) were detected in the stem cells cultured for 12 days (the samples were taken at days 0, 3, 6, 9, and 12). PCA of the lipid species (Figure S8, Supporting Information) shows that day 0 and day 3 form a cluster (termed as early adipogenesis), while the results from days 6, 9, and 12 formed another cluster (termed as late adipogenesis). Figure 7g shows the heatmap and clustering analysis (dendogram) of the top 25 lipids sorted using the VIP scores obtained from the PLS-DA. The Euclidean distance measured was plotted here, and the "Ward" algorithm for clustering was employed. Here, red shows a higher level, and blue shows a lower level of lipid species. As shown in Figure 7h, using positive ion mode, we found that the level of DGTS(6:4), DG(21:4), Cer(9:4), DGTS(15:1), and Cer(13:1) were significantly up-regulated in the stem cells at early differentiation time points (day 0, day 3). We found that the level of Cer(13:2), Cer(15:1), Cer(17:0), Cer(16:4), PC(5:1), PC(6:1), PC(7:1), PC(13:0), and DGTS(9:1) were significantly up-regulated at later differentiation time

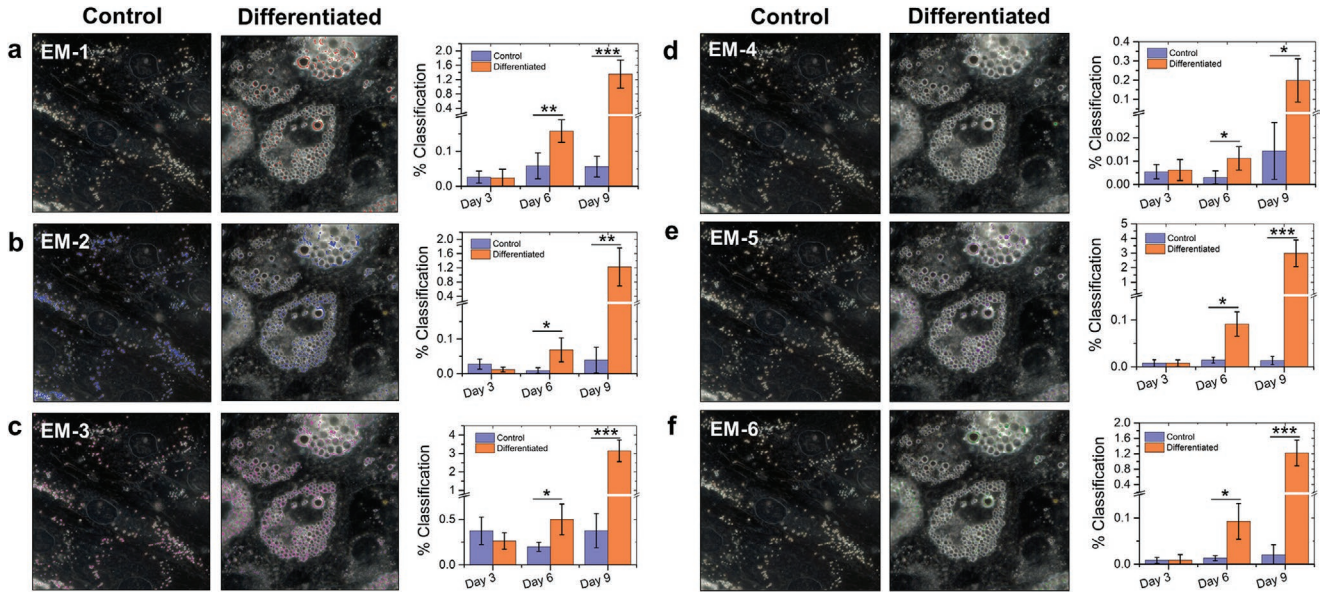

Figure 6. Comparison of Spectral Angle Mapper (SAM) analysis of the control and differentiated hASCs. Representative hyperspectral images on day 9 showing the SAM analysis of control and differentiated cells for a) end member 1 (EM-1), b) EM-2, c) EM-3, d) EM-4, e) EM-5, and f) EM-6. Histogram showing the relative percentage classification (number of matched pixels) for the control and differentiated hASCs on days 3, 6, and 9 are shown for each endmembers. The number of analyzed images was 15 for each data point, and the error bar represents the standard deviation. $*P < 0.05$, $**P < 0.01$, $***P < 0.001$, calculated using two-tailed student's *t*-test.

points (days 6, 9, 12). Different sets of lipid species were found to be up-regulated with the progression of adipogenesis using negative ion mode. For example, we found that PA(16:2), PA(16:3), PA(18:4), PE(16:0), PE(10:6), FA(27:10), and PG(12:2) were up-regulated for stem cells cultured for day 6 to day 12. Figure S9a,b (Supporting Information) show the box plot of a few of these above-identified lipid species (MG(20:9), PC(7:1), PE(12:4), PS(18:10)) indicating the differences in their normalized intensity levels.

As shown in Figure 7c, TGs are abundantly found inside the lipid droplets. TGs in adipose tissue are used for storing energy and synthesis of FAs.[39] Due to the lower oxidation states of carbons of FAs in TGs, it produces more energy than proteins or carbohydrates during oxidative metabolism. Further, due to the highly hydrophobic nature of the TGs, it does not have to carry extra hydrated water as do polysaccharides.[40] To probe the metabolic states of the differentiated hASCs, we performed multimodal (two-photon and SHG) imaging (**Figure 8**). Figure 8a–c shows the acquired images of the control cells, and Figure 8d–f shows the images of differentiated stem cells on day 9. We calculated the optical redox ratio (fluorescence intensity ratio of FAD to NADH) to understand the metabolic behavior during adipogenesis.[41] We observed a significant decrease ($P < 0.01$) of the redox ratio in the differentiated cells compared to control cells (Figure 8i,j). Meleshina et al. found a decrease in the redox ratio (FAD/NADH) during stem cell differentiation[41a,b] which they attributed to metabolic switching from glycolysis (during undifferentiated state) to oxidative phosphorylation (aerobic metabolism) during adipogenesis.[42] During glycolysis, the following reaction occurs:

$$Glucose + 2\,NAD^+ + 2ADP + 2P_i \rightarrow 2\,Pyruvate + 2\,NADH + 2H^+ + 2ATP \quad (1)$$

In this process, the FADs are not involved. The number of electrons (and energy produced, 2ATP) in glycolysis is lower than oxidative phosphorylation (34 ATP). During oxidative phosphorylation, the following reaction occurs:

$$10NADH + 10H^+ + 2FADH_2 + 34ADP + 34P_i + 6O_2 \rightarrow 10NAD^+ + 2FAD + 12H_2O + 34ATP \quad (2)$$

In oxidative phosphorylation, the number of NADH involved is increased, and the available FAD is reduced compared to glycolysis leading to a decrease in the FAD/NADH ratio.

NAD(P)H (nicotinamide adenine (pyridine) dinucleotide) and FAD (flavin adenine dinucleotide) are two co-existing enzymes that are directly related to cell metabolism. Both NAD(P)H and FAD are fluorescent in nature. Their fluorescent decay functions bear direct information on the metabolic state of the cell. The MitoTracker closely follows the fluorescent pattern of FAD. A_1 is the amplitude of the fast decay components, while A_2 is the amplitude of the slow decay component. The ratio of the amplitude of the decay components (A_1/A_2) represents the bound/unbound FAD fraction. Glycolysis yields a low A_1/A_2 for FAD, and oxidative phosphorylation yields a high A_1/A_2 for FAD. Our earlier analysis showed that the redox ratio decreases during adipogenesis differentiation. Further, it goes

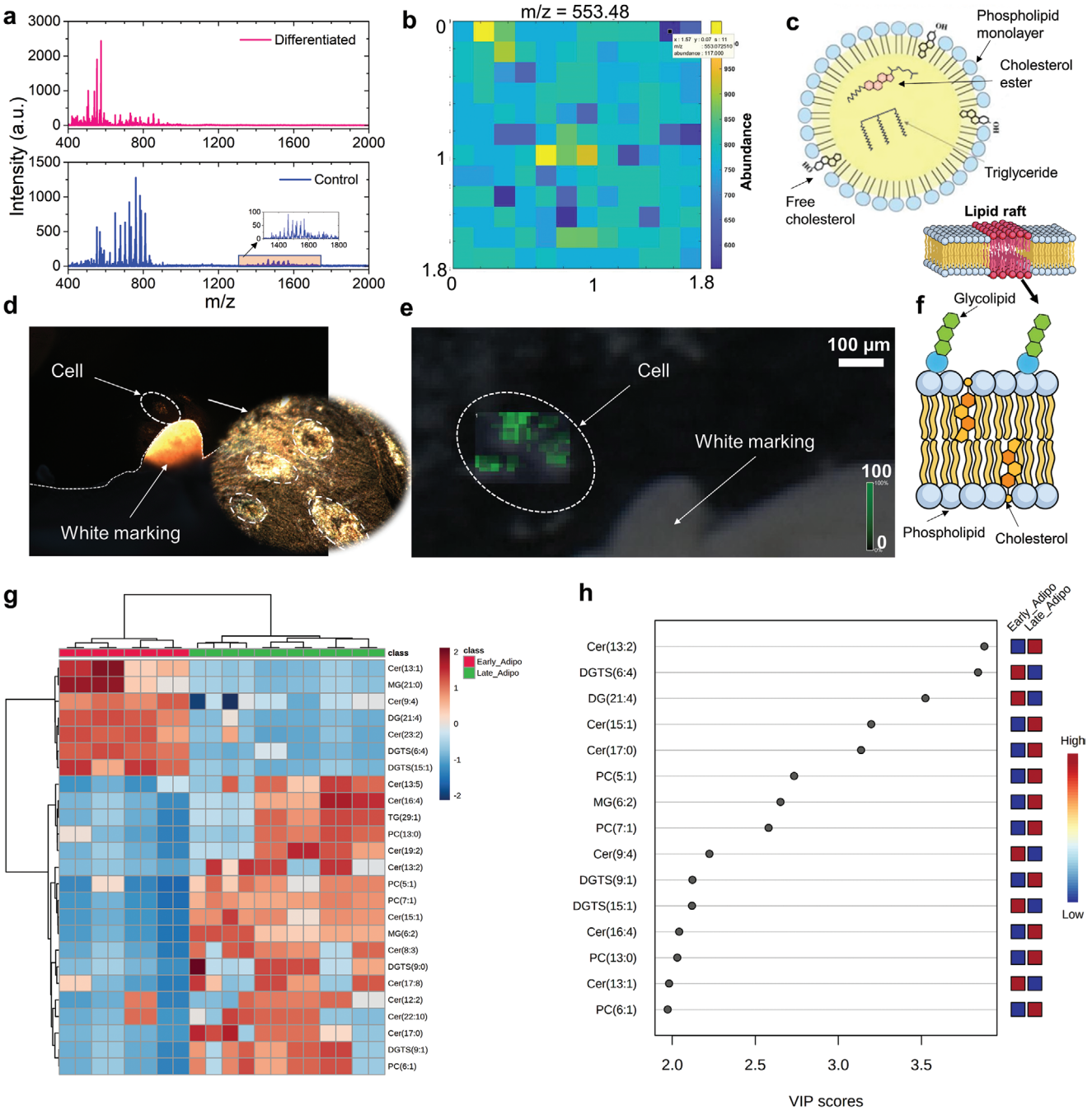

Figure 7. MALDI-MS analysis of hASCs. a) Representative MALDI-mass spectra of differentiated and control stem cells on day 9. The inset image shows peaks obtained for the control cells (m/z = 1300 – 1800), which are absent in the differentiated cells; b) A representative MALDI image of the differentiated cell at m/z = 553.48; c) schematic showing a lipid droplet and the components of the lipid droplet of the differentiated adipocytes; d) dark-field optical image of stem cell on the MALDI substrate. The inset shows the zoomed image of the cells; e) MALDI-MS image of the differentiated hADSC shown in (d), and overlaid on the respective bright-field optical image; f) schematic showing the cell membrane of a typical differentiated adipogenic stem cell. The lipid raft and the lipids found from the MALDI-MS analysis are shown in the image; g) Heatmap and cluster analysis showing top 25 lipid species that distinguishes early adipogenesis (Days 0–3) from late adipogenesis (Days 6–12) in positive ion mode; h) Partial Least Squares Discriminant Analysis (PLS-DA) showing the Variable Importance in Projection (VIP) values > 1.5 in positive ion mode at various differentiation time points (days 0–12). The colored box indicates the relative concentration of the top 15 lipid species in each group whose levels have significantly changed.

from glycolysis (during undifferentiated state) to oxidative phosphorylation (aerobic metabolism) during adipogenesis. The same trend was observed using the FLIM analysis when day 3 cells yielded a smaller A_1/A_2 ratio compared to day 6 cells (Figure 8l,m). The change in the fluorescence lifetime redox ratio (A_1/A_2) indicates a change in the cell metabolism from glycolysis to oxidative phosphorylation. After day 6, the ratio continuously decreases, implying progression in adipogenesis.

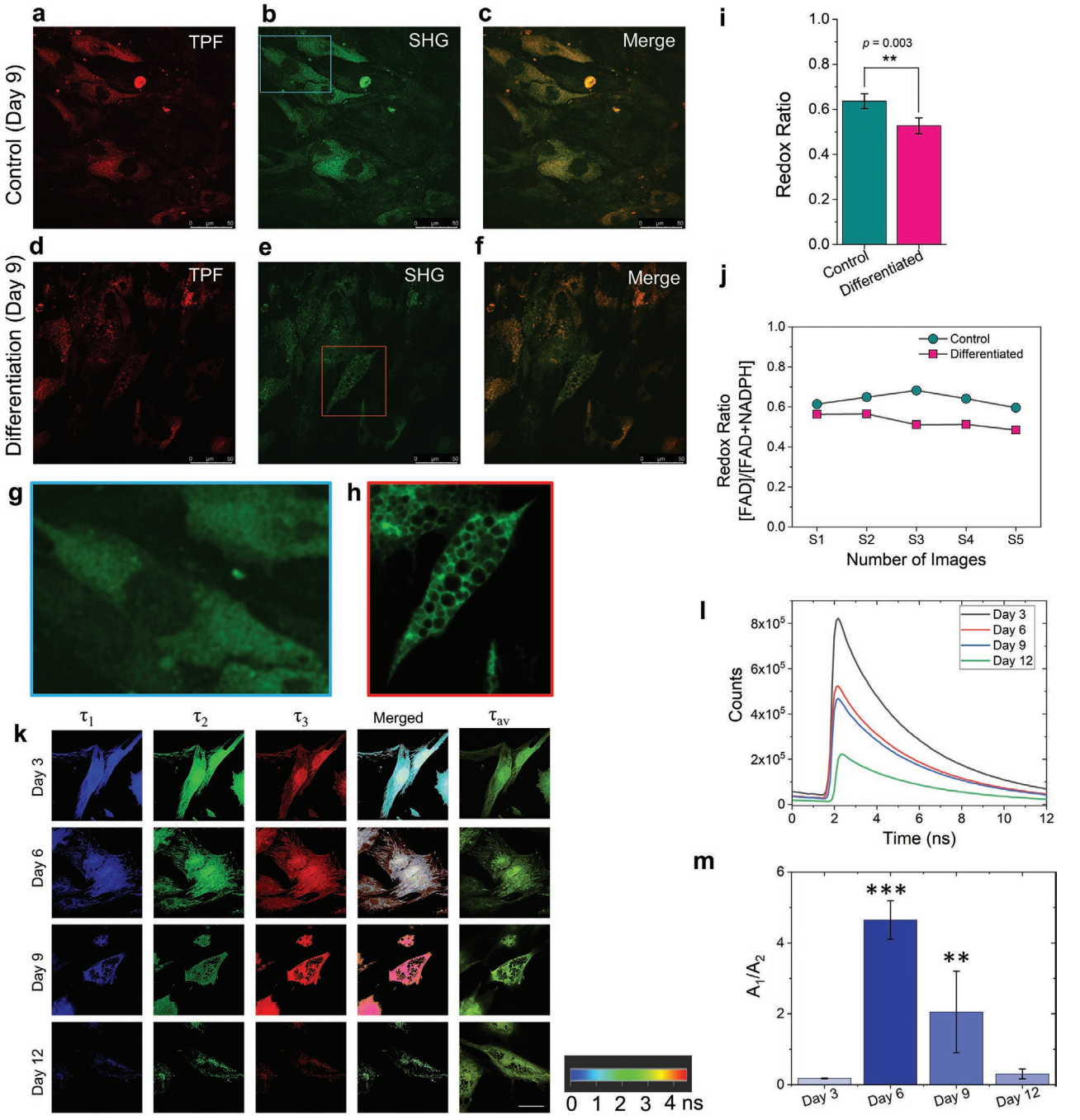

Figure 8. Metabolic imaging of the hASCs using multimodal two-photon fluorescence (TPF) and second harmonic generation (SHG) microscopy. a) TPF, b) SHG, and c) merged image of the hASCs in stromal media on day 9; d) TPF, e) SHG, and f) merged images of the hASCs in adipogenic media on day 9. The zoomed-in SHG images are shown for g) control cell (blue box in b), and h) differentiated cells (red box in e); i) comparison of optical redox ratio [FAD/(NADH+FAD)] between control and differentiated cells; j) redox ratio calculated for 5 different images corresponding to control and differentiated hASCs is shown. $^{**}P < 0.01$, calculated using two-tailed Student's *t*-test; k) Emission is captured between 584 to 622 nm. τ_1, τ_2, τ_3 represent fluorescence emissions spectrum decay components measured in nanoseconds. Pixels are pseudo-colored with R G B channel colors based on their decay times measured by the detector. The fastest component is colored blue, while the longest is colored red, as shown in a scale bar; l) photon counts of τ_{mean} (amplitude weighted) components of different differentiation days (3, 6, 9, and 12) plotted against time in nanoseconds, and m) represents amplitude ratio of fluorescence-lifetime redox ratios of amplitude-1 (A_1) and amplitude-2 (A_2).

The raw data extracted from the FLIM images of Figure 8k are presented in Table S3 (Supporting Information).

To further investigate the molecular changes during adipogenesis, we obtained Raman spectra of control and differentiated cells (**Figure 9**). Figure 9a compares the average Raman spectrum obtained from control and differentiated hASCs on day 9. Both the control and differentiated cells showed typical vibrational signatures of different cellular components[16,19a,43] such

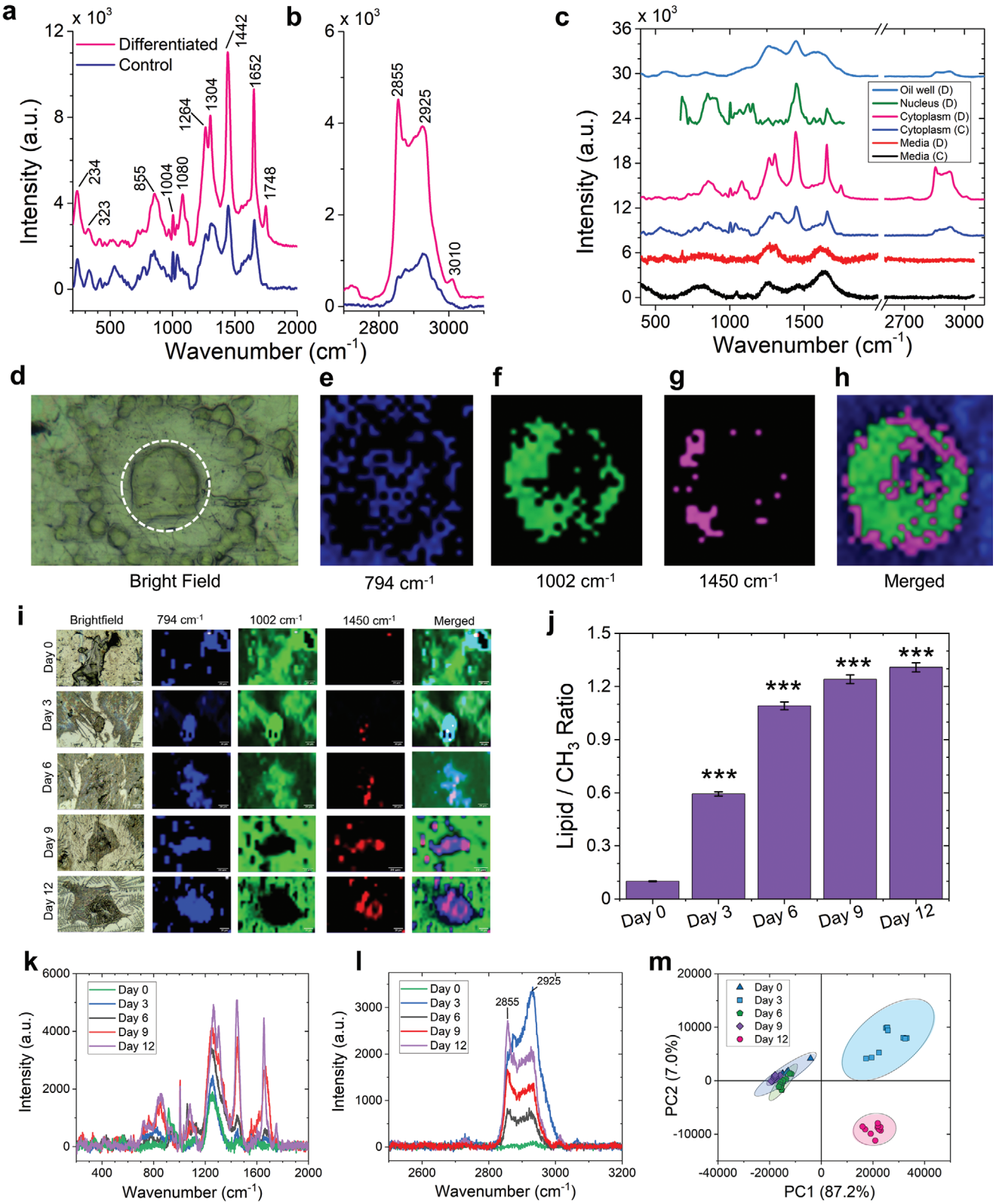

Figure 9. Raman spectroscopy and imaging of hASCs. The average Raman spectra of control and differentiated stem cells from a) 400–2000 cm^{-1}, and b) 2700–3200 cm^{-1}; c) the representative spectral signature from the sub-cellular component of a differentiated (D), and control (C) hADSC on day 9. The corresponding d) bright field image and Raman image of a single cell at specific vibrational peaks are shown in e–h; i) representative mapping data comparing bright-field images to Raman image of a single cell at specific vibrational peaks at 794 cm^{-1} (nucleic acid), 1002 cm^{-1} (amino acid), 1450 cm^{-1} (lipids). This is the low-wavenumber range; j) Represents $I_{2855}(Lipid)/I_{2925}(-CH_3)$ ratio of the differentiated cells. The average Raman spectra of the differentiated stem cells from k) 200 to 2000 cm^{-1} and l) 2500 to 3200 cm^{-1}, while m) PCA analysis of 10 spectrum collected at each differentiation day.

as proteins (1264, 1304 cm^{-1}, N-H, C-H band for amide III; 1654 cm^{-1}, amide I/α-helix), amino acids (855 cm^{-1}, tyrosine; 874 cm^{-1}, tryptophan; 1004 cm^{-1}, phenylalanine), nucleic acids (788 cm^{-1}, O-P-O stretch, 1098 cm^{-1}, PO_2 stretch), and carbohydrates (1080 cm^{-1}, C-O stretch). Here, we focused our analysis on the vibrational signature of lipids. We were able to identify three different classes of lipids (TGs, phospholipids, and CEs) using Raman spectroscopy. The characteristic C=O vibration of the ester group (1748 cm^{-1}) was seen in the differentiated cells in Figure 9a (due to a large number of lipid droplets) but not in the control cells. The intensity of vibration due to acyl chains (CH_2 bending at 1442 cm^{-1} and CH_2 twisting at 1304 cm^{-1}) was greater in the differentiated cells than control cells (Figure 9a). The peak at 1442 cm^{-1} is also attributed to phospholipids. The vibrational signatures of TGs (855 cm^{-1}) due to C-O-O and CH_3 rocking and C=O (1748 cm^{-1}) were seen in the differentiated cells. The intense peak at 1652 cm^{-1} corresponds to C=C stretching due to unsaturated lipid bonds. The C-C stretch at 1080 cm^{-1} is due to the presence of cholesterol and was found to be higher in differentiated cells due to the efficient formation of lipid droplets. The symmetric stretching mode vibration for $=CH_2$ at 2855 cm^{-1} was dramatically larger for the differentiated cells than the control due to the lipid droplet formations during adipogenesis (Figure 9b). Hence, this vibrational peak at 2855 cm^{-1} can be used to identify lipid droplets.[5,19d] The peak at 2925 cm^{-1} is due to $-CH_3$ stretching and corresponds to saturated lipid bond vibration. We calculated the $I_{2855}(Lipid)/I_{2925}(-CH_3)$ ratio of control cells to be 0.55, and the ratio for the differentiated cells was found to be 1.15. Hence, I_{2855}/I_{2925} can be utilized as a signature of adipogenesis. A significant difference between control and differentiated cells was found in the ratio between cholesterol ester (CE) and free cholesterol (FC), $I_{1748}(CE)/I_{721}(FC)$. The I_{1748}/I_{721}ratio for the differentiated cells was 2.86, and for control cells, it was 0.33. We did not find a significant difference between the unsaturated lipid to saturated lipid ratio for control and differentiated cells. $I_{1652}(C=C)/I_{1442}(-CH_2)$ signifies the ratio of unsaturated to saturated lipid content. The I_{1652}/I_{1442} for differentiated cells was 0.8 and that of control cells was 0.82. Figure 9c shows the representative spectral signature from the sub-cellular component of a differentiated (D), and control (C) hADSC on day 9. The corresponding bright-field image of the cell is shown in Figure 9d. Raman images of the cell at 794 cm^{-1} (nucleic acid, Figure 9e), 1002 cm^{-1} (amino acid, Figure 9f), 1450 cm^{-1} (lipids, Figure 9g), and the merged image (Figure 9h) are also shown. We considered the ratio of intensities for $I_{2855}(Lipid)/I_{2925}(-CH_3)$ as the signature of adipogenesis. This signature gradually increases over time from day-0 to day-12. We observed two-fold increase in the ratio when cell progressed differentiation potential from day-3 to day-6. Overall, the results demonstrate that the multimodal approach can identify the stem cell induction to adipogenesis at the single-cell level. The developed method provides a non-destructive, label-free, and cost-effective way of analyzing stem cells.

Figure 10a shows the experimental design schematically to study ex vivo implants in transgenic mice. After successfully removing the transplant, we used second harmonic generation (SHG) and HSI to explore the abundance of adipocytes in the ex vivo tissue sample. Figure 10b,c shows the SHG and two-photon (λ_{ex} = 800 nm) image of the tissue sample containing the adipocytes. The extracellular matrix (green), non-adipocytes or adipogenic cells of the recipient (circular structures), and adipocytes (circular structure with red color identifying tdTomato) are visible. To excite is tdTomato, we used a single photon laser with λ_{ex} = 561 nm. The FACS results in Figure 10d show the fraction of cells containing tdTomato. Figure 10e,f shows the HSI images of the adipocytes in the same tissue sample. Finally, Figure 10g shows the classification of differentiated and control cells in the tissue sample using the HSI spectral angle mapping algorithm. Figure 10 clearly shows that HSI can evaluate the abundancy of adipocytes derived from transplanted cells. The cells used in the study are adipocytes derived from tdTomato+ (Pdgfra lineage) adipose stem cells. tdTomato expression is permanent even after differentiation, and Pdgfra is no longer expressed in the cell. Those tdTomato+ non-adipocytes are the Pdgfra lineage cells that did not differentiate into adipocytes. Also, because of the location of transplantation, many adipogenic cells of the recipient infiltrated into the transplant and differentiated into adipocytes. The utility of HSI was further tested by evaluating its performance to distinguish adipose and osteogenic stem cells (Figures S5 and S7d, Supporting Information). The differences in the end members predicted by assessing more than 400 000 spectra in each image clearly showed that HSI is capable of distinguishing osteogenic and adipose stem cells. The HSI imaging of osteogenic stem cells was further validated using Raman microscopy (Figure S6, Supporting Information), multiphoton imaging (Figure S7a, Supporting Information), and fluorescence imaging (Figure S7b, Supporting Information).

3. Conclusion

In this study, we have demonstrated the use of HSI to identify differentiated hASCs from non-differentiated cells using the endogenous optical and spectral signatures generated from the stem cells. The HSI results were validated using traditional characterization (Oil Red O, qPCR) as well as MALDI-MS, Raman, and multiphoton imaging. The HSI method provides better resolution and contrasts to observe lipid droplets during adipogenesis than the conventional Oil Red O staining method. The label-free spectroscopy and chemical imaging methods effectively identified the chemical cues of differentiating stem cells at different days of culture in vitro and ex vivo in a transgenic mice model. The results presented here demonstrate that HSI and other label-free methods can provide quantitative molecular imaging information relevant to stem cell biology and therapies superior to conventional imaging techniques.

4. Experimental Section

hASCs Isolation: All the cell isolation and culture materials were obtained from Sigma-Aldrich (St. Louis, MO) and Fisher Scientific (Hampton, NH). Cell culture protocols used here were approved by the Western Institutional Review Board or the Pennington Biomedical Research Center (PBRC) Institutional Research Board. The cells were isolated from lipoaspirate tissues from unidentified patients with informed consent. Within 24 h of surgery, the adipose tissues were

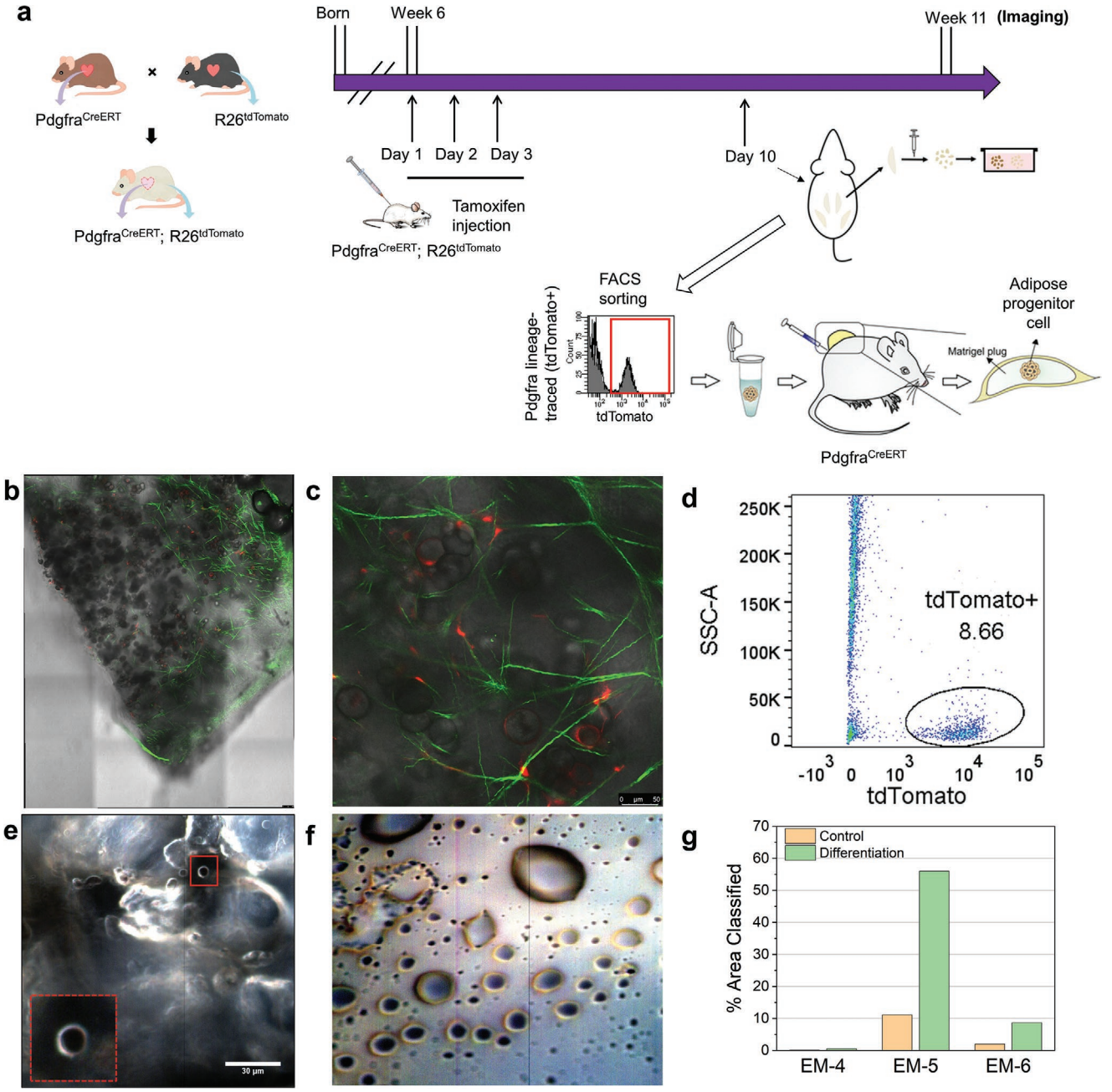

Figure 10. Ex vivo imaging of adipocytes using HSI. a) Schematic showing the experimental design to study ex vivo implant in transgenic mice. Second harmonic generation (SHG) and hyperspectral imaging (HSI) of adipocytes in the ex vivo tissue sample. b,c) SHG and two-photon (λ_{ex} = 800 nm) image of the tissue sample containing the adipocytes. The extracellular matrix (green), non-adipocytes or adipogenic cells of the recipient (circular structures), and adipocytes (circular structure with red color identifying tdTomato) are clearly visible. To excite is tdTomato, we used a single photon laser with λ_{ex} = 561 nm. d) FACS results showing the fraction of cells containing tdTomato (adipose stem cells). e,f) HSI image showing the adipose stem cells in the tissue sample. g) Classification of differentiated and control cells in the tissue sample using the HSI spectral angle mapping algorithm.

thoroughly washed with phosphate-buffered saline (PBS) solution to remove white blood cells (WBCs) and erythrocytes. The PBS solution was warmed to 37 °C, and the washing steps were repeated four times. Detailed cell isolation and culture processing procedures are available elsewhere.[4d,44] After isolation, the cells were centrifuged at (300 g) for 5 min at 25 °C to separate the remaining collagenase material. Finally, the cell pellets were cultured in the stromal medium at 37 °C, 5% CO_2, and 95% relative humidity.

Adipogenic and Osteogenic Differentiation: Adipogenesis was attained by incubating the cells with adipogenic inductive media (ADIPOQUAL, LaCell LLC, LA, USA). The adipogenic induction media was replaced every 3 days for 10 days. The adipogenic induction media contains IBMX, rosiglitazone, pantothenate, biotin, bovine insulin, penicillin, and dexamethasone. hASCs were treated with osteogenic medium (OSTEOQUAL, LaCell LLC, New Orleans, LA) for 21 days to induce osteogenesis. The media were changed every 3 days. The stromal media

used for control samples contains DMEM with 1% antibiotic and 10% FBS.

FACS Analysis: A flow cytometer (BD FACS Calibur) was utilized to characterize stem cell marker expression of hASCs at passage 2 (P2). The flow cytometry results were analyzed using Cellquest software. ASCs are stained with isotype controls and with antibody fluorophore conjugates CD29-PE, CD34-PE, CD31-Alexa Fluor CD29/CD44, CD44-FITC, CD34/CD105, CD45-PE, CD73-FITC, CD73/CD45 647, CD90/CD31, CD90-FITC, CD105-FITC, CD146-PerCP-Cy5.5. All the antibody combinations such as CD34/CD105, CD73/CD45, CD90/CD31, and CD146/CD29/CD44 were prepared as per the manufacturer's protocol (BD Biosciences). Incubation time was 20 min at 4°C for each antibody combination. The total number of cells was 10^5. The unbound antibodies were removed by centrifugation. Before performing flow cytometry (BD Biosciences, CA, USA), the cell pellets were suspended in a solution containing (1%) paraformaldehyde. For each analysis number of cells was at least 10^4.

RNA Isolation qPCR: RNAs from the stem cells were obtained employing a PureLink RNA Mini Kit (Thermo Fisher Scientific, MA, USA) and quantified using a Nanodrop spectrophotometer. cDNA was synthesized using a High-Capacity cDNA Reverse Transcription Kit (Thermo Fisher Scientific, MA, USA). Real-time quantitative polymerase chain reaction (qPCR) was performed on an ABI-7900 qPCR machine using the SYBR Green Real-Time PCR Master Mixes (Thermo Fisher Scientific, MA, USA) kit. The primer sequence for the adipogenic genes and cyclophilin B were taken from the literature.[45] The fold change in the gene expression was obtained by normalizing it with the housekeeping gene cyclophilin B and quantified using $2^{-\Delta\Delta C_T}$ method.[46]

Oil Red O Staining: hASCs cultured with and without adipogenic media at different stages (3, 6, and 9 days) were washed in PBS and were fixed in (4%) paraformaldehyde for 30 min at room temperature. After fixation, the PBS rinse step was repeated one more time, followed by treatment with (60%) isopropanol for 5 min. which is then aspirated, followed by incubating 15 min with the Oil Red O solution. A working solution of Oil Red O prepared with 3 parts of Oil Red O stock solution ((0.5%) in isopropanol) and 2 parts of distilled water made fresh was used for the staining. The Oil Red O stained cells were washed 2–3 times with PBS, and the optical images were captured at 10x magnification and analyzed using ImageJ software. After thresholding for the desired color and hue in ImageJ, images were analyzed based on area and intensity after selecting the region of interest (Figures S1–S3, Supporting Information).

Fluorescence Imaging: The cultured control and differentiated hASCs at different stages (0, 3, and 6 days) were fixed in (4%) paraformaldehyde, permeabilized with 0.2% TritonX-100 in PBS for 5 min, blocked with 0.2% fish skin gelatin (FSG), and stained with phalloidin (Ex: 488/Em: 510 nm), and counterstained with Hoechst (Ex: 460/Em: 490 nm) for fluorescence imaging. hASCsfor day 9 were fixed, permeabilized, blocked, and stained with Nile red (Ex: 530/Em: 585 nm) and counterstained with Hoechst (Ex: 460/Em: 490 nm). Phalloidin stains the cytoskeletal/actin while Nile Red acts as a marker for the mature adipocytes.[47] The concentration of the dye solution was (1 μg mL^{-1}), and the incubation time was 15 min at room temperature. The imaging was performed with a confocal fluorescence microscope (Leica TCS SP8, 63x /1.20 NA water immersion) and analyzed using ImageJ.

The following dyes were used for the fluorescence imaging of osteogenic stem cells. *Hoechst* (Blue) is a nucleus staining dye that binds to the adenosine and thymine region of DNA; *Phalloidin* (Green) is a cytoskeleton staining dye; *Runx2* (red) dye was used to stain early osteogenesis. Runx2 was found to be upregulated in immature osteoblasts (Figure S7b-iii (Supporting Information) at Week 1) and downregulated in mature osteoblasts (Figure S7b-vii (Supporting Information) at Week 2). Runx2 typically characterizes osteoblast commitment. It is co-localized around the nucleus as seen in the images; *Osteocalcin* (red spots) is a bone-forming protein; the presence of mature osteoblasts can be detected by immunostaining with osteocalcin.

Dark-Field Hyperspectral Imaging (HSI): For the HSI experiments, a CytoViva Hyperspectral Microscope with spectral imaging modality in the visible near-infrared range (λ = 400–1000 nm) was used. The high-intensity halogen light source is focused at oblique angles through the liquid light guide for efficient illumination for high contrast imaging in dark field mode. A spectral resolution of 2 nm and spatial pixel width of 25 nm was achieved using the dark-field system. Oil objectives with 100x magnification were used in the experiment in order to obtain high-resolution images. A polarizing filter was placed between the condenser and glass substrate in order to minimize random glare. Stem cells were directly grown on an ultra-cleaned glass substrate (Schott), and a coverslip was placed on the cells (fixed in place using nail polish) before imaging. Exposure time for each pixel was set to 0.30 s. The intensity of the hyperspectral spectrograph was adjusted between 1000 and 10 000 counts in order to minimize noise and avoid saturation of the images. Images were processed using ENVI 4.8 software (CytoViva) in dark-field mode.[48] Spectral information of control and differentiating hASCs obtained from experiments were normalized to 1 for analysis. In the hyperspectral images, each pixel contains the spectrum as a vector. The wavelength range or the spectral bands represent the dimension of the vector. The SAM algorithm compares the vector of each pixel for the control and differentiated stem cells with that of the vector of endmember spectrum for classification.

For HSI imaging of osteogenic differentiation, a (3 μL) solution was drop-cast on the glass substrate, and sandwich structure was generated by placing the coverslip over it. Sealing was performed using a colorless nail polish in order to prevent oil interaction (for oil objectives). Light is projected from the bottom via a high-intensity halogen lamp. Osteogenic differentiation is stimulated via solution containing glycerophosphate, L-ascorbic acid 2-phosphate sesquimagnesium salt hydrate, and dexamethasone. Based on literature and experimental observation, maturity for osteogenic differentiated stem cells is attained at day-21 compared to day-9 for adipogenesis. Hyperspectral spectra comparison of endmembers (1–4) between mature adipogenesis and osteogenesis exhibit significant differences between intensity distribution and peak positions over the 400–1000 nm wavelength range.

HSI Data Processing: Data preprocessing mainly consisted of registration of images, background subtraction, and dataset normalization. Normalization of data (with respect to the highest intensity in the VNIR spectrum) converted the radiance of HSI observations into reflectance or absorbance.[28] In order to compare each pixel in the selected field of view (FOV), the spectral angle mapper (SAM) algorithm was employed. The SAM algorithm is not sensitive to the intensity of illumination from a halogen bulb. In order to normalize the recorded vectors, dark values of the collected data were removed, and radiance values were converted to absorbance before using angle mapping as represented in the following equation:[28]

$$-\log \frac{I_{\text{sample}}}{I_{\text{lamp spectrum}}} = I_{\text{absorbance}} \tag{3}$$

In each pixel of endmember and sampler data cubes, the value of the n^{th} dimension is the distance between reference origin and the intensity value within that n^{th} band. A simple vector multiplication between the inverse matrix of the endmember library and the observed mixed/unknown spectrum gives an estimate of the distribution of the library endmembers in the unknown spectrum. Results for the SAM classification, in turn, produce an image showing the best match at each pixel. Results are usually presented as a grayscale image with values ranging from 0 to 1, which corresponds to the relative degree of the match. The best spectral match occurs when the angle between the vectors is the smallest, i.e., 0. In this study, threshold limits of θ were restricted to ± 0.15. Therefore, the unknown spectrum is classified as a "match" to the known spectrum if the angles were smaller than the threshold value. The angle within the spectral match was obtained using the following relationship:[49]

$$\theta = \frac{180}{\pi} \cos^{-1}\left[\frac{\vec{s} \times \vec{r}}{\| \vec{s} \| \times \| \vec{r} \|}\right] \tag{4}$$

where $\vec{s}$ and $\vec{r}$ are sample and reference, respectively. All the images were calibrated for illumination and reflectance such that the SAM

classification was insensitive to albedo or lamp effects. The percentage pixel match data was further weighted based on the area with biomatrix in the FOV.

Mass Spectrometry of hASCs Using Matrix-Assisted Laser Ionization/Deposition (MALDI) Imaging and Liquid Chromatography-Mass Spectrometry (LC-MS): hASCs were grown on indium tin oxide (ITO) coated slides (UniversityWafer Inc, MA, USA). All chemicals for matrix preparation, such as methanol, LC-MS grade water, and DHB (2, 5-dihydroxybenzoic acid), were procured from Sigma-Aldrich (St. Louis, MO) while TFA (trifluoroacetic acid) from Fisher Scientific (Atlanta, GA, USA). The matrix solution was prepared with a 1:1 ratio of LC-MS grade water and methanol, containing 0.1% v/v TFA and up to (10 mg mL^{-1}) of DHB. In order to thoroughly mix solute into the solvent, vortexing was employed for 5 min. The slides were vacuum dried for 10 min before matrix deposition. An in-house built pneumatic sprayer with compressed gas (N_2) at a pressure of 10 psi was used to spray the matrix at the rate of (50 µL min^{-1}) on the cells. Approximately (0.5 mL) of DHB matrix was used to deposit a uniform layer (spray plus dry cycles coating) over the cells fixated on the ITO slides. Immediately after DHB deposition, the slides were heated under a lamp for 10 min until the liquid matrix crystallized. MALDI-MS imaging spectra were acquired using a MALDI-TOF/TOF mass spectrometer (UltrafleXtreme, Bruker Daltonics, Billerica, MA, USA) with 5 ppm mass accuracy. The system was calibrated externally using a well-known 5-peptide mix drop cast on the sample slide with a 1:1 ratio by volume to the matrix. Optical bright-field and dark-field images of the samples were taken before matrix deposition for proper calibration via FlexImaging software (Bruker). Each spectrum was produced from 25 laser shots per spot within selected regions of interest (ROI) with a step size of 10 µm. Laser shots were fired in spot-array over the 0.05 mm^2 area. Spectra were recorded in positive ion mode in the mass range 400–2000 *m/z*. MALDI-MS imaging spectra were evaluated using BrukerFlex Analysis 3.0 software and MSiReader (open-source Matlab package) [50] after baseline subtraction using a B-spline fit.

Liquid chromatography-mass spectrometric (LC-MS) measurements were conducted on two different systems. Pelleted samples were lysed by adding (250 µL) of LC-MS grade methanol and vortexing for 1 min. Cell lysates were incubated at room temperature on an orbital shaker at 500 rpm for 30 min before adding (250 µL) of LC-MS grade water. Cell debris was pelleted by centrifugation at 12 000 rpm for 10 min, and supernatants were transferred to new microcentrifuge tubes. Each tube was added with (500 µL) of HPLC grade chloroform, vortexed for 1 min, and incubated at room temperature on an orbital shaker at 500 rpm for 30 min. The organic layer was transferred to a new tube and evaporated under a gentle stream of nitrogen. Samples were then reconstituted in (65 µL) of (30%) ACN solution containing (0.1%) formic acid. LC-MS analyses were conducted on an Agilent 1260 Infinity II quaternary liquid chromatography coupled to an Agilent 6230 electrospray time-of-flight mass spectrometer (Agilent, Santa Clara, CA). Samples were run with a capillary voltage of 4000 V. Nitrogen was used as drying gas delivered at (10 L min^{-1}) at a temperature of 325 °C, and the fragment voltage was set to 150 V. The mass range used was 100–3000 *m/z*. An Agilent Poroshell 120 EC-C18 column (2.7 mm ID, 150 mm length, 2.7 µm pores, end-capped) was used for chromatographic separation with a gradient program using a binary mixture of mobile phases at a fixed flow rate of 400 µL min^{-1}. Mobile phases composition was as follows: A = 0.1% formic acid in H_2O, and B = acetonitrile. The gradient program was as follows: 0–5 min = 5% B, 5–30 min 90%B, 30–35 min 90%B, 35–45 min 5% B. A volume of (30 µL) was used for each injection, and samples were run both in positive as well as in negative mode. LC-MS samples were exported to mzData file format with MassHunter Workstation module Qualitative Analysis Navigator (Ver. B.08.00, Build 8.0.8208.0). Further data analysis and lipid database search were conducted with MZMine 2 and MetaboAnalyst 5.0.

Multiphoton Microscopy of hASCs, Osteogenic Stem Cells, and Ex Vivo Tissue Containing Adipocytes: The two-photon fluorescence (TPF) and second harmonic generation (SHG) images of the hASCs were obtained using a Leica SP5 resonant scanning multiphoton confocal microscope with a Spectra Physics Mai-Tai femtosecond tunable pulsed near-IR laser (690 – 1040 nm). A 63x oil objective was used for the image acquisition. The endogenous fluorescence from nicotinamide adenine dinucleotides hydrogen (NADH) and flavin adenine dinucleotides (FAD) [51] were generated by using a Ti: Sa femtosecond laser, with 4000 MHz repetition rate and 70 fs pulse duration. For NADH, an excitation wavelength of 750 nm was used and emission was collected using a filter of 320–430 nm. For FAD, an excitation wavelength of 860 nm was used and an emission filter of 486 – 506 nm. The redox ratio of FAD/(NADH+FAD) was calculated at each pixel using ImageJ analysis.[52]

SHG and two-photon images of the tissue sample containing the adipocytes were obtained at λ_{ex} = 800 nm. To excite is tdTomato, a single photon laser with λ_{ex} = 561 nm was used. The osteogenic stem cells were imaged using SHG in a way similar to that of hASC imaging described above.

Fluorescence Lifetime Imaging Microscopy of hASCs: To perform metabolic imaging in the stem cells, the mitochondria of the cells were labelled by incubating the differentiated cells with MitoTracker fluorescent probes, which accumulate in active mitochondria by passively diffusing across the cellular plasma membrane. After the cellular mitochondria are tagged, the differentiated cells are treated with an aldehyde-based fixative such as para-formaldyhyde to process the sample further. Diluted 1×10^{-3} M MitoTracker stock solution is mixed with the final dyeing concentration in the appropriate buffer or growth medium. For staining for the adipogenesis differentiated cells that are to be fixed and permeabilized, a working concentration of 200×10^{-9} M was used. Then the media was removed from the well-plate containing cells and pre-warmed (37 °C) staining solution containing MitoTracker probe solution was added. Incubation for 15–45 min was performed. Then medium/buffer covering the differenitated cells was carefully pipetted out and was replaced with newly prepared, pre-warmed buffer or growth medium that contains 4% formaldehyde. After fixing the cells, it was rinsed multiple times in the PBS buffer. FLIM data were captured using Leica TCS SP8 confocal microscope with motorized DIC accessories. Super sensitive hybrid detectors remove reflected light and autofluorescence. A white light laser at 561 nm excited the stem cell samples via a 63x/1.20 water immersion objective. Line repetitions are set at count 4 while frame repetitions at count 3. The image size was 144.72 µm x 144.72 µm, and the tandem scanner speed was 700 Hz, corresponding to frame rate 0.057 s^{-1}. Pixel size 141.47 nm x 141.47 nm with dwell time 762 ns. Emission was captured between 584 to 622 nm.

Raman Imaging of hASCs and Osteogenic Differentiated Cells: The Raman spectra and images of the hASCs were obtained using a Raman microspectroscope system (Renishaw inVia Reflex Raman Spectroscopy, UK) at a magnification of 50x (long working distance). Laser excitation of 785 nm was used with an exposure time of 20 s in the wavenumber range of 200–3200 cm^{-1} for acquiring the spectra. For the Raman maps, the Map Image Acquisition mode of the system was used. For the Raman images, the following configuration was utilized: grating of 1200 l mm^{-1} (633/780), integration time of 2 s, wavenumber range of 665–1773 cm^{-1}, and static mode centered on 1250 cm^{-1}. All the Raman spectra were calibrated against the silicon peak at 520 cm^{-1}.

Raman Spectroscopy and microscopy of control versus differentiated osteogenic cells were performed for weeks 1, 2, and 3. The experiment was done with 785 nm laser, 100% power, magnification of 50x (long distance), 1200 grating, and exposure time of 10 s for spectral acquisition and 0.5 s for map acquisition.

Statistical Analysis: For calculating the *P*-value (statistical significance), a two-tailed Student's *t*-test or one-way ANOVA was used. Principal component analysis (PCA) was performed using Origin (OriginLab, MA, USA). All the data were expressed in terms of mean and standard deviation.

In Vivo Implantation of adipocytes: *Pdgfra* CreERT (JAX#03 2770) and *R26* tdTomato(JAX#0 07909) mice crossed to generate *Pdgfra* CreERT*; R26* tdTomato mice. Six week old male *Pdgfra* CreERT*; R26* tdTomato mice were treated with tamoxifen for 3 days by intraperitoneal injection (100 mg kg^{-1} body weight/day) to induce the expression of tdTomato in *Pdgfra* lineage-traced cells. One week after the last tamoxifen injection,

epididymal adipose tissue was removed for cell isolation by enzymatic digestion. *Pdgfra* lineage-traced (tdTomato$^+$) adipose progenitor cells were sorted from tissue slurry using a FACSAria sorter (BD Biosciences). 4000 cells were mixed with (30 µL) Matrigel and injected into the subcutaneous space in the mid-back of WT mouse. The transplant was removed 3 weeks after injection. All experiments involving mice were approved by the Institutional Animal Care and Use Committee (IACUC) at Louisiana State University (approval numbers IACUC 19-011 and 20-061).

Supporting Information

Supporting Information is available from the Wiley Online Library or from the author.

Acknowledgements

Raman and fluorescence experiments were performed at LSU's Shared Instrumentation Facility (SIF). SHG experiments were performed at the Genomics or Cell Biology & Bioimaging core facilities that are supported in part by COBRE (NIH8 1P30GM118430-01) and NORC (NIH 1P30-DK072476) center grants from the National Institutes of Health. M.R.G. acknowledges National Science Foundation (NSF CAREER award number: 2045640), LSU start-up fund, and Louisiana Board of Regents Support Fund (RCS Award Contract Number: LEQSF (2017-20)-RD-A-04). AC is supported by LSU Economic Development Assistantships (EDA). X.F. is supported by NIH grant 1R15DK122383. The authors thank Dr. David Burk for the help with the fluorescence and SHG experiments. RD acknowledges support from the LSU Alumni Professorship and from NIH 1R01DE024790 and 1R15GM141653.

Conflict of Interest

The authors declare no conflict of interest.

Data Availability Statement

Research data are not shared.

Keywords

hyperspectral imaging, label-free stem cell imaging, MALDI, Raman microscopy, second harmonic generation

Received: April 26, 2021
Revised: July 11, 2021
Published online:

[1] A. I. Caplan, *J. Orthop. Res.* **1991**, *9*, 641.
[2] D. Baksh, R. Yao, R. S. Tuan, *Stem Cells* **2007**, *25*, 1384.
[3] J. M. Gimble, F. Guilak, *Cytotherapy* **2003**, *5*, 362.
[4] a) L. Wu, T. Wang, Y. Ge, X. Cai, J. Wang, Y. Lin, *Cell Proliferation* **2012**, *45*, 311; b) A. S. Greenberg, M. S. Obin, *Am. J. Clin. Nutr.* **2006**, *83*, 461S; c) G. Fantuzzi, *J. Allergy Clin. Immunol.* **2005**, *115*, 911; d) S. Shaik, X. Wu, J. Gimble, R. Devireddy, *Sci. Rep.* **2018**, *8*, 8162.
[5] I. R. Suhito, Y. Han, J. Min, H. Son, T.-H. Kim, *Biomaterials* **2018**, *154*, 223.
[6] a) H. Hentze, P. L. Soong, S. T. Wang, B. W. Phillips, T. C. Putti, N. R. Dunn, *Stem Cell Res.* **2009**, *2*, 198; b) A. S. Lee, C. Tang, F. Cao, X. Xie, K. van der Bogt, A. Hwang, A. J. Connolly, R. C. Robbins, J. C. Wu, *Cell Cycle* **2009**, *8*, 2608.
[7] P. C. Smits, R.-J. M. van Geuns, D. Poldermans, M. Bountioukos, E. E. Onderwater, C. H. Lee, A. P. Maat, P. W. Serruys, *J. Am. Coll. Cardiol.* **2003**, *42*, 2063.
[8] T. Kuroda, S. Yasuda, S. Kusakawa, N. Hirata, Y. Kanda, K. Suzuki, M. Takahashi, S.-I. Nishikawa, S. Kawamata, Y. Sato, *PLoS One* **2012**, *7*, 37342.
[9] a) J. J. Cunningham, T. M. Ulbright, M. F. Pera, L. H. Looijenga, *Nat. Biotechnol.* **2012**, *30*, 849; b) H. Okano, M. Nakamura, K. Yoshida, Y. Okada, O. Tsuji, S. Nori, E. Ikeda, S. Yamanaka, K. Miura, *Circ. Res.* **2013**, *112*, 523; c) B. Lu, C. Malcuit, S. Wang, S. Girman, P. Francis, L. Lemieux, R. Lanza, R. Lund, *Stem Cells* **2009**, *27*, 2126.
[10] a) I. R. Suhito, N. Angeline, S.-S. Choo, H. Y. Woo, T. Paik, T. Lee, T.-H. Kim, *Sensors* **2018**, *18*, 2755; b) P. O. Bagnaninchi, N. Drummond, *Proc. Natl. Acad. Sci. USA* **2011**, *108*, 6462; c) C. Hildebrandt, H. Büth, S. Cho, H. Thielecke, *J. Biotechnol.* **2010**, *148*, 83.
[11] C. Molony, J. McIntyre, A. Maguire, R. Hakimjavadi, D. Burtenshaw, G. Casey, M. Di Luca, B. Hennelly, H. J. Byrne, P. A. Cahill, *Biochim. Biophys. Acta, Mol. Cell Res.* **2018**, *1865*, 343.
[12] J.-X. Cheng, X. S. Xie, *Science* **2015**, *350*, aaa8870.
[13] J. P. Smus, C. C. Moura, E. McMorrow, R. S. Tare, R. O. Oreffo, S. Mahajan, *Chem. Sci.* **2015**, *6*, 7089.
[14] E. Sarró, M. Lecina, A. Fontova, F. Gòdia, R. Bragós, J. J. Cairó, *J. Chem. Technol. Biotechnol.* **2016**, *91*, 1755.
[15] A. Downes, R. Mouras, A. Elfick, *J. Biomed. Biotechnol.* **2010**, *2010*, 101864.
[16] C. Kallepitis, M. S. Bergholt, M. M. Mazo, V. Leonardo, S. C. Skaalure, S. A. Maynard, M. M. Stevens, *Nat. Commun.* **2017**, *8*, 14843.
[17] a) J. Sulé-Suso, N. Forsyth, V. Untereiner, G. Sockalingum, *Trends Biotechnol.* **2014**, *32*, 254; b) S. Gomathy, C. Stylianou, I. Phang, S. Cool, V. Nurcombe, F. Ample, M. Lear, S. Gorelik, J. Hobley, presented at *2010 Photonics Global Conf.*, Photonics Global Conference, Singapore **2010**; c) J. R. Beattie, S. E. Bell, C. Borggaard, A. M. Fearon, B. W. Moss, *Lipids* **2007**, *42*, 679.
[18] a) L. L. McManus, G. A. Burke, M. M. McCafferty, P. O'Hare, M. Modreanu, A. R. Boyd, B. J. Meenan, *Analyst* **2011**, *136*, 2471; b) L. L. McManus, F. Bonnier, G. A. Burke, B. J. Meenan, A. R. Boyd, H. J. Byrne, *Analyst* **2012**, *137*, 1559; c) A. Hashimoto, Y. Yamaguchi, C. Morimoto, K. Fujita, M. Takedachi, S. Kawata, S. Murakami, E. Tamiya, *Sci. Rep.* **2015**, *5*, 12529; d) S. J. Smith, R. Emery, A. Pitsillides, C. E. Clarkin, S. Mahajan, *Analyst* **2017**, *142*, 1962.
[19] a) F. C. Pascut, S. Kalra, V. George, N. Welch, C. Denning, I. Notingher, *Biochim. Biophys. Acta, Gen. Subj.* **2013**, *1830*, 3517; b) T.-H. Kim, K.-B. Lee, J.-W. Choi, *Biomaterials* **2013**, *34*, 8660; c) J. Marzi, E. M. Brauchle, K. Schenke-Layland, M. W. Rolle, *Acta Biomater.* **2019**, *89*, 193; d) A. F. Palonpon, M. Sodeoka, K. Fujita, *Curr. Opin. Chem. Biol.* **2013**, *17*, 708; e) T. C. von Erlach, M. A. Hedegaard, M. M. Stevens, *Analyst* **2015**, *140*, 1798; f) A. Ghita, F. C. Pascut, M. Mather, V. Sottile, I. Notingher, *Anal. Chem.* **2012**, *84*, 3155.
[20] K. J. Ember, M. A. Hoeve, S. L. McAughtrie, M. S. Bergholt, B. J. Dwyer, M. M. Stevens, K. Faulds, S. J. Forbes, C. J. Campbell, *NPJ Regener. Med.* **2017**, *2*, 12.
[21] M. S. Patterson, B. C. Wilson, D. R. Wyman, *Lasers Med. Sci.* **1991**, *6*, 155.
[22] Y. Xu, S.-H. Mirmalek-Sani, F. Lin, J. Zhang, R. O. Oreffo, *RNA* **2007**, *13*, 1179.
[23] Y. Fu, N. Luo, R. L. Klein, W. T. Garvey, *J. Lipid Res.* **2005**, *46*, 1369.
[24] B. Venugopal, F. B. Fernandez, V. Harikrishnan, A. John, *J. Mater. Sci.: Mater. Med.* **2017**, *28*, 28.

[25] S. Farmer, *Int. J. Obes.* **2005**, *29*, S13.
[26] a) J. Zhang, H. Tang, Y. Zhang, R. Deng, L. Shao, Y. Liu, F. Li, X. Wang, L. Zhou, *Int. J. Mol. Med* **2014**, *33*, 1209; b) N. Haider, L. Larose, *Cell Commun. Signaling* **2020**, *18*, 26.
[27] M. I. Lefterova, A. K. Haakonsson, M. A. Lazar, S. Mandrup, *Trends Endocrinol. Metab.* **2014**, *25*, 293.
[28] G. Lu, B. Fei, *J. Biomed. Opt.* **2014**, *19*, 010901.
[29] a) E. J. Lanni, S. S. Rubakhin, J. V. Sweedler, *J. Proteomics* **2012**, *75*, 5036; b) D. S. Cornett, M. L. Reyzer, P. Chaurand, R. M. Caprioli, *Nat. Methods* **2007**, *4*, 828.
[30] J.-S. Ryu, K.-T. Chang, J.-T. Lee, M.-U. Lim, H.-K. Min, Y.-J. Na, S.-B. Lee, G. Moussavou, S.-U. Kim, J.-S. Kim, *BMB Rep.* **2012**, *45*, 713.
[31] M. Frick, C. Schmidt, *Chem. Phys. Lipids* **2019**, *221*, 145.
[32] a) C. Lipina, H. S. Hundal, *FEBS Lett.* **2015**, *589*, 3221; b) J.-i. Inokuchi, K.-i. Inamori, K. Kabayama, M. Nagafuku, S. Uemura, S. Go, A. Suzuki, I. Ohno, H. Kanoh, F. Shishido, in *Progress in Molecular Biology and Translational Science*, Elsevier, New York Vol. *156*, **2018**, p. 151; c) J. M. Wentworth, G. Naselli, K. Ngui, G. K. Smyth, R. Liu, P. E. O'Brien, C. Bruce, J. Weir, M. Cinel, P. J. Meikle, *Int. J. Obes.* **2016**, *40*, 706.
[33] E. G. Sustarsic, T. Ma, M. D. Lynes, M. Larsen, I. Karavaeva, J. F. Havelund, C. H. Nielsen, M. P. Jedrychowski, M. Moreno-Torres, M. Lundh, *Cell Metab.* **2018**, *28*, 159.
[34] J. N. van der Veen, J. P. Kennelly, S. Wan, J. E. Vance, D. E. Vance, R. L. Jacobs, *Biochim. Biophys. Acta Biomembr.* **2017**, *1859*, 1558.
[35] a) M. Almena, I. Mérida, *Trends Biochem. Sci.* **2011**, *36*, 593; b) L. S. de Sá Barretto, C. Lessio, A. N. S. e Nakamura, E. G. L. Turco, C. G. da Silva, J. P. Zambon, F. C. Gozzo, E. J. Pilau, F. G. de Almeida, *In Vitro Cell. Dev. Biol.:Anim.* **2014**, *50*, 831.
[36] W. Christie, *The Lipid Library*, Elsevier, New York **2013**.
[37] C.-H. Tung, M. S. Han, J. Qi, *PLoS One* **2017**, *12*, 0179158.
[38] M. Maceyka, S. Spiegel, *Nature* **2014**, *510*, 58.
[39] K. Czamara, K. Majzner, M. Z. Pacia, K. Kochan, A. Kaczor, M. Baranska, *J. Raman Spectrosc.* **2015**, *46*, 4.
[40] D. L. Nelson, A. L. Lehninger, M. M. Cox, *Lehninger Principles of Biochemistry*, Macmillan, New York **2008**.
[41] a) A. V. Meleshina, V. V. Dudenkova, M. V. Shirmanova, V. I. Shcheslavskiy, W. Becker, A. S. Bystrova, E. I. Cherkasova, E. V. Zagaynova, *Sci. Rep.* **2016**, *6*, 21853; b) A. V. Meleshina, V. V. Dudenkova, A. S. Bystrova, D. S. Kuznetsova, M. V. Shirmanova, E. V. Zagaynova, *Stem Cell Res. Ther.* **2017**, *8*, 15; c) O. I. Kolenc, K. P. Quinn, *Antioxid. Redox Signaling* **2019**, *30*, 875; d) K. P. Quinn, G. V. Sridharan, R. S. Hayden, D. L. Kaplan, K. Lee, I. Georgakoudi, *Sci. Rep.* **2013**, *3*, 3432; e) A. Varone, J. Xylas, K. P. Quinn, D. Pouli, G. Sridharan, M. E. McLaughlin-Drubin, C. Alonzo, K. Lee, K. Münger, I. Georgakoudi, *Cancer Res.* **2014**, *74*, 3067.
[42] C. D. Folmes, P. P. Dzeja, T. J. Nelson, A. Terzic, *Cell Stem Cell* **2012**, *11*, 596.
[43] a) D. I. Ellis, D. P. Cowcher, L. Ashton, S. O'Hagan, R. Goodacre, *Analyst* **2013**, *138*, 3871; b) A. Ditta, H. Nawaz, T. Mahmood, M. Majeed, M. Tahir, N. Rashid, M. Muddassar, A. Al-Saadi, H. Byrne, *Spectrochim. Acta, Part A* **2019**, *221*, 117173.
[44] S. Shaik, D. Hayes, J. Gimble, R. Devireddy, *Stem Cells Dev.* **2017**, *26*, 608.
[45] J. Li, F. Zanata, J. L. Curley, E. C. Martin, X. Wu, M. Dietrich, R. V. Devireddy, J. W. Wade, J. M. Gimble, *Cells Tissues Organs* **2016**, *201*, 14.
[46] K. J. Livak, T. D. Schmittgen, *Methods* **2001**, *25*, 402.
[47] W. Zhao, X. Li, X. Liu, N. Zhang, X. Wen, *Mater. Sci. Eng., C* **2014**, *40*, 316.
[48] N. Mehta, A. Mahigir, G. Veronis, M. R. Gartia, *in Plasmonics: Design, Materials, Fabrication, Characterization, and Applications*, International Society for Optics and Photonics, Bellingham, WA **2017**, p. 1034631.
[49] S. S. More, R. Vince, *ACS Chem. Neurosci.* **2015**, *6*, 306.
[50] a) G. Robichaud, K. P. Garrard, J. A. Barry, D. C. Muddiman, *J. Am. Soc. Mass Spectrom.* **2013**, *24*, 718; b) M. T. Bokhart, M. Nazari, K. P. Garrard, D. C. Muddiman, *J. Am. Soc. Mass Spectrom.* **2017**, *29*, 8.
[51] a) B. Chance, R. W. Estabrook, A. Ghosh, *Proc. Natl. Acad. Sci. USA* **1964**, *51*, 1244; b) R. Scholz, R. G. Thurman, J. R. Williamson, B. Chance, T. Bücher, *J. Biol. Chem.* **1969**, *244*, 2317.
[52] K. P. Quinn, E. Bellas, N. Fourligas, K. Lee, D. L. Kaplan, I. Georgakoudi, *Biomaterials* **2012**, *33*, 5341.